Society For Biomaterials

The effect of local IL-4 delivery or CCL2 blockade on implant fixation and bone structural properties in a mouse model of wear particle induced osteolysis

Taishi Sato,[1*] Jukka Pajarinen,[1*] Anthony Behn,[1] Xinyi Jiang,[1] Tzu-hua Lin,[1] Florence Loi,[1] Zhenyu Yao,[1] Kensuke Egashira,[2] Fan Yang,[1,3] Stuart B. Goodman[1,3]

[1]Department of Orthopaedic Surgery, Stanford University, Stanford, California
[2]Department of Cardiovascular Research, Development, and Translational Medicine, Kyushu University Graduate School of Medicine, Fukuoka, Japan
[3]Department of Bioengineering, Stanford University, Stanford, California

Received 24 February 2016; revised 25 March 2016; accepted 21 April 2016
Published online 00 Month 2016 in Wiley Online Library (wileyonlinelibrary.com). DOI: 10.1002/jbm.a.35759

Abstract: Modulation of macrophage polarization and prevention of CCL2-induced macrophage chemotaxis are emerging strategies to reduce wear particle induced osteolysis and aseptic total joint replacement loosening. In this study, the effect of continuous IL-4 delivery or bioactive implant coating that constitutively releases a protein inhibitor of CCL2 signaling (7ND) on particle induced osteolysis were studied in the murine continuous femoral intramedullary particle infusion model. Polyethylene particles with or without IL-4 were infused into mouse distal femurs implanted with hollow titanium rods using subcutaneous infusion pumps. In another experimental group, particles were infused into the femur through a 7ND coated rod. After 4 weeks, fixation of the implant was assessed using a pullout test. The volume of trabecular bone and the geometry of the local cortical bone were assessed by μCT and the corresponding structural properties of the cortical bone determined by torsional testing. Continuous IL-4 delivery led to increased trabecular bone volume as well as enhanced local bone geometry and structural properties, while 7ND implant coating did not have effect on these parameters. The results suggest that local IL-4 treatment is a promising strategy to mitigate wear particle induced osteolysis. © 2016 Wiley Periodicals, Inc. J Biomed Mater Res Part A: 00A:000–000, 2016.

Key Words: aseptic loosening, macrophage, interleukin-4, CCL2, bone structural properties

How to cite this article: Sato T, Pajarinen J, Behn A, Jiang X, Lin T-H, Loi F, Yao Z, Egashira K, Yang F, Goodman SB. 2016. The effect of local IL-4 delivery or CCL2 blockade on implant fixation and bone structural properties in a mouse model of wear particle induced osteolysis. J Biomed Mater Res Part A 2016:00A:000–000.

INTRODUCTION

Aseptic loosening remains one of the main long-term complications of total joint replacement (TJR) surgery. Peri-implant osteolysis and subsequent loosening of TJRs are driven by macrophage-mediated inflammation to implant-derived ultra-high molecular weight polyethylene (UHMWPE) and other biomaterial wear particles.[1,2] Wear particle-activated macrophages secrete chemokines and pro-inflammatory cytokines that lead to further macrophage recruitment, increased osteoclastogenesis, and suppression of osteoblast function.[3,4] Together these changes create a microenvironment that favors bone resorption over formation, ultimately leading to periprosthetic osteolysis. Currently, no pharmacological therapies have been successfully used clinically to mitigate this process; the only treatment available for the advanced cases is revision surgery. However, novel treatment options targeting the inflammatory pathways and, in particular, the particle-induced macrophage activation and macrophage homing to the area of inflammation are emerging.[5]

One such strategy to limit wear particle induced osteolysis is the local modulation of macrophage polarization. Macrophages are a dynamic population of cells that can assume multiple functional phenotypes as guided by the local microenvironment; inflammatory M1 macrophages, induced by lipopolysaccharide (LPS) and/or interferon gamma (IFN-γ), and tissue regenerative M2 macrophages induced by interleukin-4 (IL-4) represent the extremes of this

*These authors contributed equally to this work.
Correspondence to: S. B. Goodman; e-mail: goodbone@stanford.edu
Contract grant sponsor: NIH; contract grant numbers: 2R01 AR055650, 1R01AR063717, R01DE024772
Contract grant sponsor: California Institute for Regenerative Medicine; contract grant number: RT3-07804
Contract grant sponsor: National Science Foundation CAREER Award Program; contract grant number: CBET-1351289
Contract grant sponsors: Ellenburg Chair in Surgery in Stanford University; 3M Nontenured Faculty Grant; Stanford Chem-H Institute; Jane and Aatos Erkko Foundation; Stanford Child Health Research Institute

macrophage activation continuum.[6,7] Biomaterial wear particles activate macrophages into inflammatory, M1-like, phenotype characterized by production of proinflammatory cytokines and chemokines. In contrast, several studies have shown that induction of M2 macrophage polarization by IL-4 prevents biomaterial particle-induced macrophage activation and inflammation *in vitro*.[8–10] Corresponding results were reported using a mouse calvarial model in which local IL-4 injections significantly reduced UHMWPE particle-induced inflammation and osteolysis by modulating local macrophage phenotype.[11]

Among the inflammatory chemokines that wear debris-activated macrophages produce, the role of CCL2 (Monocyte Chemoattractant Protein-1, MCP-1) is especially well established.[12] Indeed retrieval studies have shown that the peri-implant tissue expresses high levels of CCL2, which has been shown to play a central role in the systemic recruitment of macrophages to the area of particle induced inflammation *in vitro* and *in vivo*.[13–15] Furthermore, blockade of CCL2 signaling with specific antibody reduced both systemic macrophage homing and local osteolysis in the murine continuous femoral intramedullary particle infusion model.[14] Reducing macrophage homing to the peri-implant tissue by preventing the action of CCL2 thus constitutes another emerging approach to limit particle induced osteolysis.

CCL2 signals through C-C chemokine receptors 2 and 4 (CCR2/CCR4) expressed on monocyte/macrophages. 7ND is a mutant version of CCL2 protein that lacks the amino acids 2 through 8 from its N-terminal end and has been shown to function as an inhibitor of CCL2 signaling.[16–18] Recently it has been shown that 7ND prevents not only particle-induced macrophage chemotaxis but also particle-induced inflammation *in vitro*.[19] Similar results were obtained using the mouse calvarial model in which local injections of 7ND effectively mitigated particle induced osteolysis.[20] Based on these results a biodegradable surface coating that constitutively releases biologically active 7ND was recently developed to prevent particle-induced osteolysis.[21]

In this study, the murine continuous femoral intramedullary particle infusion model[14,22–24] was used to explore the effect of local IL-4 delivery or 7ND releasing implant coating on the implant fixation and the structural properties of the surrounding bone. It was hypothesized that these treatments would prevent particle-induced osteolysis leading to improved implant fixation and enhancement of the structural properties of the local bone.

METHODS

7ND-releasing surface coating

Titanium rods were coated with a biodegradable, 7ND-releasing coating following a previously established layer-by-layer (LBL) method.[21] Briefly, end-modified poly(β-amino ester) (C32-130) was synthesized as previously described, suspended in phosphate buffered saline (PBS) at 10 mg mL^{-1} and used as the positively charged polyelectrolyte. A 3 mg mL^{-1} polystyrene sulfonate was used as the negatively charged polyelectrolyte. The 7ND was dissolved in 0.1% (w/v) bovine serum albumin at 30 μg mL^{-1}. Prior to coating hollow A-40 titanium rods (6 mm, 21 G, New England Small Tube, Litchfield, NH) were surface etched with concentrated hydrochloric acid (37.3% w/v, Fisher Scientific, Pittsburgh, PA) for 2 h to facilitate the attachment of the coating. Rods were then thoroughly washed with H_2O, rinsed three times in 70% ethanol, air dried, and subjected the LBL deposition, with polyelectrolyte layers on bottom and the 7ND containing layer on top. Polyelectrolyte layers were deposited for 5 min, and the 7ND layer for 10 min. In between layer depositions rods were washed twice in H_2O. The sustained release of 7ND from the surface coating was confirmed *in vitro* using CCL2 ELISA (Peprotech, Rocky Hill, NJ) as previously described.[21]

UHMWPE particles and osmotic pumps

Conventional UHMWPE particles were a generous gift from Dr. Timothy Wright, Hospital for Special Surgery. Particles were isolated from knee joint simulator test supernatants according to established protocols.[14] Following isolation particles were washed twice in ethanol (96%, 70%) and, after evaporation of ethanol, suspended in PBS for storage in −80°C. The particles tested negative for endotoxin using a Limulus Amebocyte Lysate Kit (BioWhittaker, Walkersville, MD). The mean diameter of the particles was 0.48 ± 0.10 μm as measured by electron microscopy. Alzet model 2006 (Durect Corporation, Cupertino, CA) osmotic pumps were loaded either with carrier solution (1% BSA-PBS); carrier solution with 15 mg mL^{-1} UHMWPE particles; or carrier solution with UHMWPE particles and 10 μg mL^{-1} mouse recombinant IL-4 (R&D Systems, Minneapolis, MN). 6-cm-long vinyl tubing (Durect Corporation), prefilled with the appropriate solution, was used to connect the pumps to the coated or noncoated titanium rods.[22]

Mouse model of wear particle induced osteolysis and experimental groups

The murine continuous femoral intramedullary particle infusion model was performed as previously described.[14,23,24] The study was carried out in strict accordance with the recommendations in the Guide for the Care and Use of Laboratory Animals of the National Institutes of Health. The protocol was approved by the Administrative Panel on Laboratory Animal Care (APLAC) at Stanford University. Briefly, the right distal femur of 48, 10- to 12-week-old male BALB/cByJ mice (The Jackson Laboratory, Bar Harbor, ME) under isoflurane inhalation anesthesia was exposed by performing a lateral parapatellar arthrotomy. An axial drill-hole was created though the intercondylar notch to access medullary cavity using a series of needles and the titanium rod, with or without 7ND-releasing coating, was subsequently press-fit into the distal femur at mean depth of 3 mm [Fig. 1(a,b)]. Osmotic pumps were then implanted in the subcutaneous tissue on the left-dorsal side of the mouse and a subcutaneous tunnel reaching the right knee was created to connect the tubing to the implanted rod. Four experimental groups were defined, each with 12 mice randomly assigned to the groups: (1) Pumps with carrier solution, uncoated rod; (2) pumps with UHMWPE particles, uncoated rod; (3)

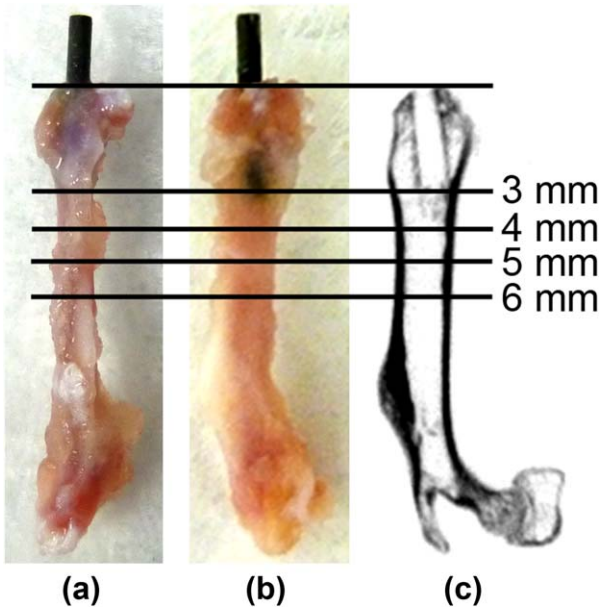

FIGURE 1. Location of the implant in the mouse distal femur. UHMWPE particles with or without IL-4 or 7ND releasing implant surface coating were infused into murine distal femurs through a hollow titanium rod, axially press fit to a mean depth of 3 mm through the intercondylar region. (a) Lateral and (b) posterior views of the femurs excised 4 weeks after the implantation showing the rod *in situ*. (c) Corresponding coronal plane μCT image after the rod removal with pullout test. The footprint of the implant is evident in the distal epi- and metaphyseal region. Horizontal lines show the location of μCT transverse sections chosen for the detailed μCT image analysis 3, 4, 5, 6 mm from the distal end of the femur.

pumps with UHMWPE particles, 7-ND releasing rod; (4) Pumps with UHMWPE particles and IL-4, uncoated rod. Skin incisions were closed with 5–0 Ethilon sutures and repeated subcutaneous buprenorphine injections were used in the postoperative analgesia. Mice were individually housed at Stanford University animal housing facilities in a temperature-controlled environment on a 12-h light-dark cycle. Food and water were provided ad libitum. Four weeks after the surgery mice were euthanized, the left and right femora were collected and stored in −80°C. On the day of testing, specimens were thawed in PBS and kept moist throughout the imaging and testing. The mechanical testing and imaging was performed during one day to eliminate potential effects of freeze-thaw cycles.

Implant pullout test

Pullout testing was performed on a Model 5944 Materials Testing System using a 100 N load cell (Instron Corporation, Norwood, MA). Prior to testing, digital calipers were used to measure the length of the rod protruding from the distal end of the femur. Each specimen was mounted to the testing machine by placing the exposed rod through a hole in a loading platform with the condyles pressed against the underside of the platform. The platform was secured to a three-axis tilting vise mounted to an xy stage. The position and angular alignment of the platform was adjusted in order to make the titanium rod coaxial with the test machine pull axis. The exposed rod was then secured in a drill chuck attached in-line with a universal joint to the test machine actuator. The universal joint aided in specimen alignment and reduced off axis loading [Fig. 2(a)]. Following preloading to 1 N, the rod was pulled a rate of 1 mm min^{-1} until failure.[25] Force and displacement were recorded at 100 Hz. Embedded surface area (SA) was determined by multiplying the embedded rod length by the rod circumference. Interfacial shear strength was defined as the maximum pullout force divided by SA. Apparent shear stiffness was defined as the slope of the linear portion of the shear stress versus displacement curve. Displacement calculations were adjusted to account for the test set-up compliance. Following rod removal via pullout testing, the proximal and distal ends of the femur were potted in polymethylmethacrylate (PMMA) and secured in a radiolucent Delrin blocks. A custom fixture was used to center the femur in the potting blocks and ensure proper diaphyseal axis alignment. The contralateral (left) femurs were potted using the same procedure.

μCT and image analysis

All femurs were imaged with an eXplore Locus RS150 MicroCT (GE Healthcare, Fairfield,CT). The 49 μm scans

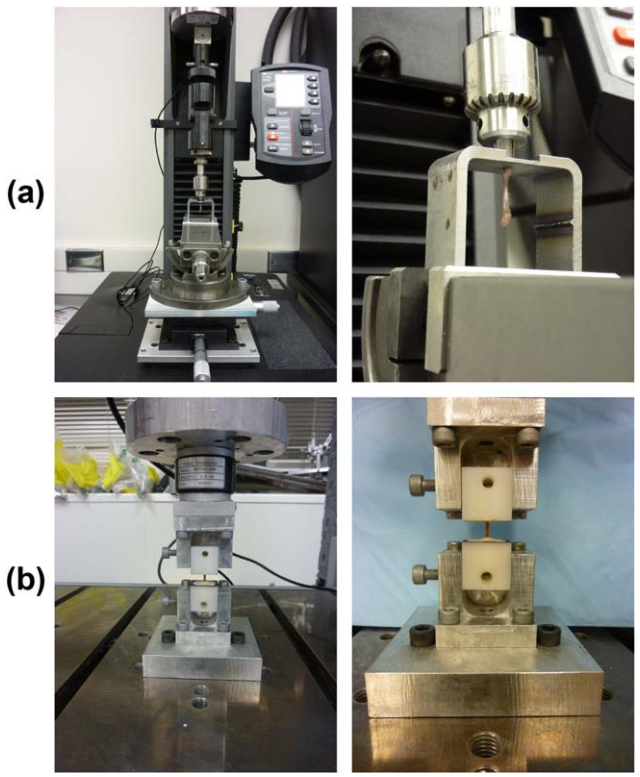

FIGURE 2. Experimental set-ups used for implant pullout and torsion tests. (a) During pullout testing, the implanted titanium rods were placed through a hole in a loading plate while the femoral condyles were set against the underside of the plate. Alignment of the rod was achieved by adjusting a tilting vise and xy stage. The rod was clamped in a drill chuck placed in-line with a universal joint. (b) During torsion testing, the proximal and distal potting blocks were secured to the test machine with the diaphyseal axis aligned with the rotation axis of the materials test machine.

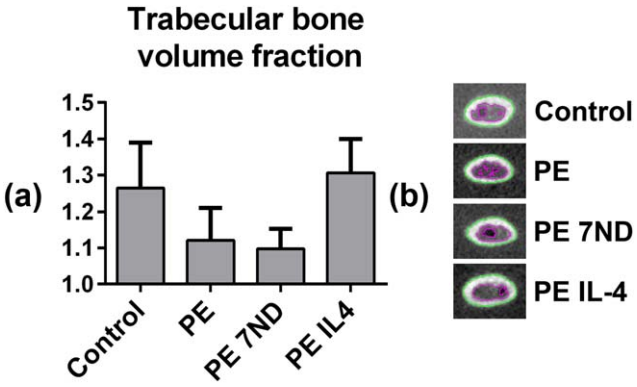

FIGURE 3. The volume fraction of trabecular bone in the distal femur as determined by μCT. UHMWPE particles with or without IL-4 or 7ND releasing implant surface coating were infused into murine distal femurs through a hollow titanium rod implanted to a mean depth of 3 mm. (a) After 4 weeks the volume fraction of trabecular bone from 4 to 5 mm from the distal end of the femur was determined from consecutive transverse plane μCT images. (b) Transverse plane μCT images showing the segmentation of trabecular and cortical bone at ~4 mm from the distal end of the femur. Green line tracks the borders of the cortical bone and the purple line borders of trabecular bone region. Note the large amount of bone in the IL-4 treated group.

were performed with 120 kVp, two frames per view, 360° rotation, and 2 × 2 binning. Specimens were submerged in PBS during imaging. Images were calibrated against a calibration phantom of known densities (water, air, and hydroxyapatite) and initially analyzed in GEMS MicroView software. A custom MATLAB program was then used to segment the images and determine cross-sectional properties. Segmentation was accomplished using the half maximum height method.[26] The cortical area, polar moment of inertia (J), and the maximum and minimum principal bending moments of inertia (Imax, Imin) were determined from transverse plane images 3, 4, 5 and 6 mm from the distal end of the femurs [Fig. 1(c)]. The mechanically weakest bone-cross section was also defined from the transverse plane images of the whole femurs. Trabecular bone volume fraction was calculated using the inner boundary of cortical bone determined from image segmentation and by taking the ratio of trabecular bone volume to the total intramedullary volume in the region from 4 to 5 mm from the distal end of the femurs.

Torsion test

Torsional testing was conducted on an ElectroPuls E10000 Materials Testing System (Instron Corporation) equipped with a 0.2 Nm capacity torque transducer (Interface, Scottsdale, AZ) [Fig. 2(b)]. Gage length, defined as the length of the unpotted bone, was recorded with digital calipers. Specimens were preloaded to 1 Nmm and then rotated at a rate of 1 deg s^{-1} internal rotation about the diaphyseal axis of the bone until failure.[27] Torque and angular displacement were recorded at 100 Hz. Rotation measurements were adjusted to account for test set-up compliance. Angular displacement was divided by specimen gage length to obtain specimen twist (rad/mm). Torque versus twist was plotted for further analysis. Outcome measures included maximum torque and torsional rigidity (defined as the slope of the linear portion of the torque vs. twist curve). Failure location and mode were documented for each specimen.

Statistical analysis

Mice that showed abnormal weight loss during the experiment, with misaligned rods or missing data due to suboptimal μCT image quality or missing left side comparison data were excluded from the analysis. Grubbs' tests ($\alpha = 0.05$) were used to detect further outliers with the final sample size being 7 to 11 mice per group. Statistical analyses were conducted using Graphpad Prism version 6.03 (GraphPad Software, La Jolla, CA). ANOVA with Tukey's post-hoc tests were used for the statistical comparison of the experimental groups. All data except the rod pull-out results (shear strength, apparent shear stiffness) are presented as normalized values (ratio of right femur to left femur) in order to account for variations between animals. Values are presented as mean ± standard error of mean.

RESULTS

μCT and local bone geometry

The continuous infusion of the UHMWPE particles caused local trabecular bone loss evident on μCT as reduced trabecular bone volume fraction 4 to 5 mm from the distal end of the femur (Fig. 3). In contrast, wear particle infusion did not have a clear impact on the area of cortical bone or the bone geometry (I_{max}, I_{min}, and J) as compared to the control group at the investigated regions of interest (Fig. 4). The 7ND releasing implant coating was not effective in preventing the particle-induced trabecular bone loss nor did it significantly alter the cortical area or bone geometry at the investigated regions of interest (Figs. 3 and 4). In contrast, continuous IL-4 delivery with the UHMWPE particles led both to prevention of particle induced trabecular bone loss and local increase in the cortical bone area with corresponding improvement in the bone geometry 4 and 5 mm from the distal end of the bone (Figs. 3 and 4). The mechanically weakest cross-section of all the femurs was located within the proximal third of the femur at ~7 mm from the distal end of the bone, and was not affected by the treatments (not shown).

Implant pullout

The continuous delivery of the UHMWPE particles via the hollow titanium rod did not significantly impact shear strength or apparent shear stiffness of the bone-implant interface, compared to controls without particles (Fig. 5). The implants with 7ND releasing surface coating showed a trend for reduced shear strength whereas continuous IL-4 delivery did not have an impact on the pullout parameters of the implant (Fig. 5).

Torsion test

The continuous delivery of the UHMWPE particles did not significantly alter the structural properties of the femur subjected to torsional stress, as maximum torque and torsional rigidity remained unaltered compared to the controls (Fig. 6). Similarly, the 7ND coating did not have a clear

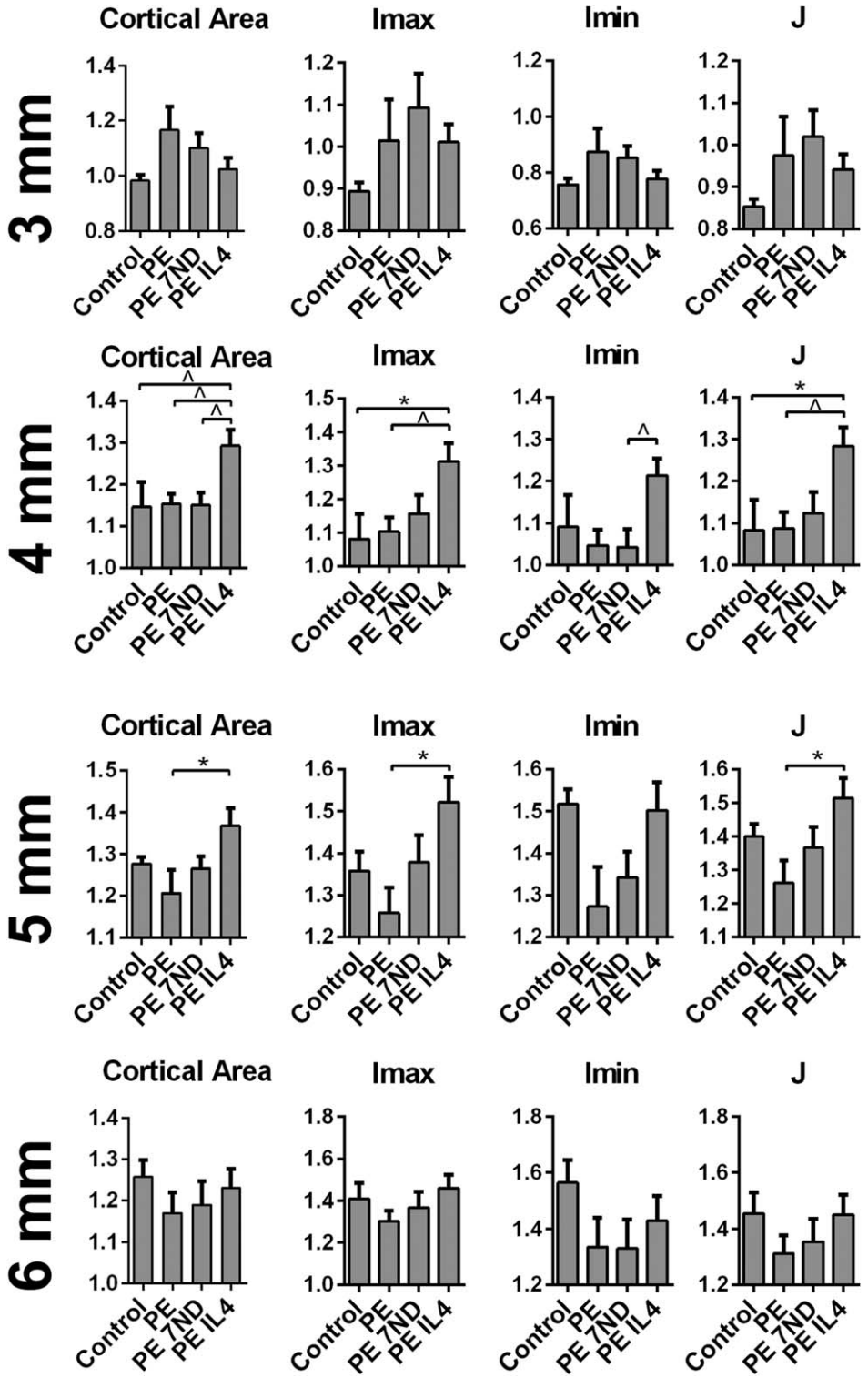

FIGURE 4. Cortical cross sectional properties of distal femur as determined by μCT. UHMWPE particles with or without IL-4 or 7ND releasing implant surface coating were infused into murine distal femurs through a hollow titanium rod implanted to a mean depth of 3 mm. After 4 weeks the normalized cortical area and bone geometry was determined from transverse plane μCT images 3, 4, 5, and 6 mm from the distal end of the femur. Imax, Imin – maximum and minimum principal bending moments of inertia; J—polar moment of inertia; $*p < 0.05$;$\hat{}p < 0.08$.

impact on the bone structural properties. In contrast, continuous IL-4 delivery led to slight increase in the torsional rigidity while maximum torque remained unaltered. All of the femora failed in a spiral fracture pattern at the mid diaphysis corresponding to the area of the mechanically weakest cross-section identified in the μCT analysis

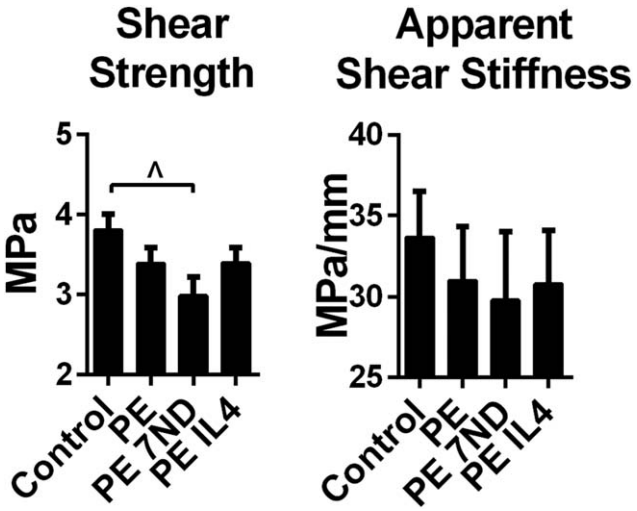

FIGURE 5. Implant fixation as determined by pullout test. UHMWPE particles with or without IL-4 or 7ND releasing implant surface coating were infused into murine distal femurs through a hollow titanium rod. After 4 weeks the fixation of the implant was assessed by pullout test and shear strength and apparent shear stiffness determined. ^$p < 0.08$.

DISCUSSION

In this study the effect of two emerging strategies to limit wear particle-induced osteolysis, namely continuous IL-4 delivery and 7ND releasing biodegradable surface coating, on implant fixation, bone geometry and the structural properties of the surrounding bone were investigated in a previously established murine continuous femoral intramedullary particle infusion model. Implant fixation was assessed by implant pullout testing with the calculation of shear strength and apparent shear stiffness. The volume fraction of the local trabecular bone and the geometry of the local cortical bone were assessed by μCT imaging with the following variables determined from the transverse plane images: cortical area, maximum and minimum principal bending moments of inertia (I_{max}, I_{min}) and polar moment of inertia (J). These variables reflect cortical bone's resistance to axial, bending, and torsional stresses, respectively. Although it is not strictly valid for noncircular cross sections, the polar moment of inertia serves as an estimation of torsional stiffness. Finally, the effects of the different treatments on the structural properties of the femora were determined by torsional testing to failure with the determination of maximum torque and torsional rigidity.

The continuous infusion of UHMWPE particles led to local trabecular bone loss although the differences between the groups did not reach statistical significance most likely due to relatively small sample size and unexpectedly high variation between the samples. Wear particles did not have a clear impact on the total area or the geometry of cortical bone at the investigated regions of interest. As the cortical bone carries most the torsional load it can be speculated that also the structural properties of the femora remained unaffected. Indeed, in the torsional test, maximum torque, and torsional rigidity of the particle treated femora were similar to the controls. Previous studies utilizing this model system have reported particle-induced ostolysis evident in μCT as a reduction of the overall bone volume fraction and/or mineral density in the distal femur.[14,23,24] These studies have not, however, compared the effect of the continuous particle delivery on the local trabecular and cortical bone. Indeed, the current study found that particle-induced osteolysis in this model occurs mainly in the metaphyseal trabecular bone with little impact on the cortical bone or overall mechanical stability of the femur that would become evident in the torsional test.

The 7ND releasing implant coating was not effective in preventing particle-induced trabecular bone loss 4 to 5 mm from the distal end of the femur. Likewise it did not alter the area of the cortical bone or the bone geometry at the investigated regions of interest, nor did it affect the corresponding bone structural properties. This might be due to the highly localized release of the 7ND limiting the effect of the drug to the immediate surroundings of the implant.

In contrast, continuous IL-4 delivery with UHMWPE particles led both to prevention of particle induced trabecular bone loss and local increase in the cortical bone area with corresponding improvement in the bone geometry. The effect was evident at 4 and 5 mm from the distal end of the femur corresponding to the immediate site of IL-4 delivery but did not extend more proximally to the region of interest defined as 6 mm from the distal end of the femur. This localized effect might suggest dilution and/or metabolism of the continuously delivered IL-4 limiting the extent of its biological effects.

The improvement of local bone geometry by IL-4 delivery was reflected by increase in the torsional rigidity, while the maximum torque remained unaffected. This can be

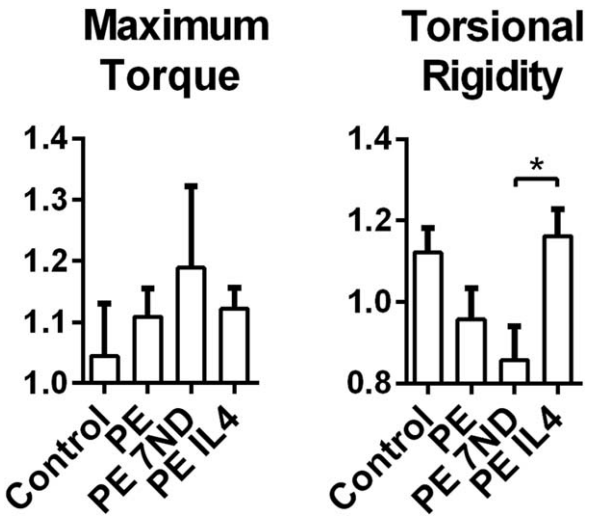

FIGURE 6. Bone structural properties as determined by torsion test. UHMWPE particles with or without IL-4 or 7ND releasing implant surface coating were infused into murine distal femurs through a hollow titanium rod. After 4 weeks the rod was removed with pullout test and the structural properties of the surrounding bone determined by torsion test. Normalized values of maximum torque before failure and torsional rigidity were determined. *$p < 0.05$.

explained by the fact that maximum torque to failure is determined by the cross-section of the femur with the least torsional resistance while torsional rigidity is influenced by the cross sectional variations along the entire length of the bone. In all of the treatment groups the cross-section of the femur with the least torsional resistance and, therefore, the expected breaking point of the bone was located ~7 mm from the distal end of the femur. Thus all the femora placed under torsional stress failed at the same location with the same maximum torque. In contrast, continuous IL-4 delivery led to local increase in the cortical area and polar moment of inertia at the distal femur that was visible in the torsion test as an increased torsional rigidity.

The exact mechanism by which continuous IL-4 delivery together with UHMWPE wear particles led to the prevention of particle-induced trabecular bone loss and local increase in the cortical area with improvement in the bone geometry remains unknown. It is tempting to speculate, however, that continuous IL-4 delivery led to local M2 macrophage polarization with reduced inflammatory response toward wear particles.[22,28] In addition to regulating macrophage phenotype it is well recognized that IL-4 inhibits osteoclast formation and function.[29] In contrast, the effects of IL-4 on bone forming cells including mesenchymal stem cells, osteoprogenitor cells, and osteoblasts are more controversial.[30,31]

Implant fixation to surrounding bone was as assessed by pullout test. The continuous infusion of UHMWPE particles with or without IL-4 did not have a clear impact on the implant fixation possibly because both the particles and IL-4 were delivered through the hollow titanium rod to its proximal end rather than directly to the bone-implant interface. Somewhat unexpectedly the 7ND releasing coating failed to improve implant fixation. At present the reason for this observation remains unknown but reduced friction at the interface due to the surface treatment might be one explanation for the phenomenon. Alternatively it is possible that similar to fracture healing, the initial inflammatory reaction and macrophage influx are necessary for optimal bone-implant integration and that inhibiting these processes is, in fact, detrimental to subsequent implant fixation.[32]

Previously the murine continuous femoral intramedullary particle infusion model has been used to study the local and systemic inflammation reaction and cell biology of the wear particle-induced osteolysis, including the systemic homing of macrophages and mesenchymal stem cells to the area of particle induced inflammation.[14,23,24,33] The aim of the current study was to extent the utility of the system to include biomechanical testing of the bone structure and implant fixation. The mechanical testing devices and protocols established for the current study will be further developed in the subsequent studies to address for the limitations encountered. For example it was unexpected that the potential effect of the particles and the treatments on the local bone mechanical properties would be masked by the fact that the weakest cross-section of the femurs and thus the expected breaking point would be at the proximal diaphysis even after the continuous infusion of wear particles to the distal femur. In future studies the assessment of the potential effect that wear particles and/or treatments have on the mechanical properties of the local bone should be focused on immediate area of particle delivery, rather than the whole length of the bone. Additionally, to better assess the effect of the particle and/or IL-4 delivery on the fixation of the implant, rods with radially directed holes may be considered to increase particle and/or IL-4 delivery directly to the implant surface.

In summary, out of the two tested strategies to prevent wear particle-induced osteolysis, the 7ND releasing implant coating did not mitigate particle-induced bone loss or improve bone structural properties. In contrast, continuous local IL-4 delivery was an effective means to prevent particle-induced bone loss and enhance bone structural properties in the context of wear particle-induced inflammation. The results suggest that local IL-4 treatment is a promising strategy to mitigate wear particle-induced inflammation and osteolysis while 7ND releasing implant coating requires further development.

ACKNOWLEDGMENTS

Imaging studies were done at Stanford Small Animal Imaging Service Center.

REFERENCES

1. Landgraeber S, Jäger M, Jacobs JJ, Hallab NJ. The pathology of orthopedic implant failure is mediated by innate immune system cytokines. Mediators Inflamm 2014;185150.
2. Pajarinen J, Lin TH, Sato T, Yao Z, Goodman S. Interaction of materials and biology in total joint replacement—Successes, challenges and future directions. J Mater Chem B Mater Biol Med 2014;2:7094–7108.
3. Ingham E, Fisher J. The role of macrophages in osteolysis of total joint replacement. Biomaterials 2005;26:1271–1286.
4. Nich C, Takakubo Y, Pajarinen J, Ainola M, Salem A, Sillat T, Rao AJ, Raska M, Tamaki Y, Takagi M, Konttinen YT, Goodman SB, Gallo J. Macrophages-Key cells in the response to wear debris from joint replacements. J Biomed Mater Res A 2013;101:3033–3045.
5. Goodman SB I, Gibon E, Pajarinen J, Lin TH, Keeney M, Ren PG, Nich C, Yao Z, Egashira K, Yang F, Konttinen YT. Novel biological strategies for treatment of wear particle-induced periprosthetic osteolysis of orthopaedic implants for joint replacement. J R Soc Interface 2014;11:20130962.
6. Mosser DM, Edwards JP. Exploring the full spectrum of macrophage activation. Nat Rev Immunol 2008;8:958–969.
7. Murray PJ, Wynn TA. Protective and pathogenic functions of macrophage subsets. Nat Rev Immunol 2011;11:723–737.
8. Trindade MC, Nakashima Y, Lind M, Sun DH, Goodman SB, Maloney WJ, Schurman DJ, Smith RL. Interleukin-4 inhibits granulocyte-macrophage colony-stimulating factor, interleukin-6, and tumor necrosis factor-alpha expression by human monocytes in response to polymethylmethacrylate particle challenge in vitro. J Orthop Res 1999;17:797–802.
9. Rao AJ, Gibon E, Ma T, Yao Z, Smith RL, Goodman SB. Revision joint replacement, wear particles, and macrophage polarization. Acta Biomater 2012;8:2815–2823.
10. Pajarinen J, Kouri VP, Jämsen E, Li TF, Mandelin J, Konttinen YT. The response of macrophages to titanium particles is determined by macrophage polarization. Acta Biomater 2013;9:9229–9240.
11. Rao AJ, Nich C, Dhulipala LS, Gibon E, Valladares R, Zwingenberger S, Smith RL, Goodman SB. Local effect of IL-4 delivery on polyethylene particle induced osteolysis in the murine calvarium. J Biomed Mater Res A 2013;101:1926–1934.
12. Goodman SB, Ma T. Cellular chemotaxis induced by wear particles from joint replacements. Biomaterials 2010;31:5045–5050.

13. Huang Z, Ma T, Ren PG, Smith RL, Goodman SB. Effects of orthopedic polymer particles on chemotaxis of macrophages and mesenchymal stem cells. J Biomed Mater Res A 2010;94:1264–1269.
14. Gibon E, Ma T, Ren PG, Fritton K, Biswal S, Yao Z, Smith L, Goodman SB. Selective inhibition of the MCP-1-CCR2 ligand-receptor axis decreases systemic trafficking of macrophages in the presence of UHMWPE particles. J Orthop Res 2012;30:547–553.
15. Jämsen E, Kouri VP, Olkkonen J, Cör A, Goodman SB, Konttinen YT, Pajarinen J. Characterization of macrophage polarizing cytokines in the aseptic loosening of total hip replacements. J Orthop Res 2014;32:1241–1246.
16. Gong JH, Clark-Lewis I. Antagonists of monocyte chemoattractant protein 1 identified by modification of functionally critical NH2-terminal residues. J Exp Med 1995;181:631–640.
17. McQuibban GA I, Gong JH, Wong JP, Wallace JL, Clark-Lewis I, Overall CM. Matrix metalloproteinase processing of monocyte chemoattractant proteins generates CC chemokine receptor antagonists with anti-inflammatory properties in vivo. Blood 2002;100: 1160–1167.
18. Egashira K, Nakano K, Ohtani K, Funakoshi K, Zhao G, Ihara Y, Koga J, Kimura S, Tominaga R, Sunagawa K. Local delivery of anti-monocyte chemoattractant protein-1 by gene-eluting stents attenuates in-stent stenosis in rabbits and monkeys. Arterioscler Thromb Vasc Biol 2007;27:2563–2568.
19. Yao Z, Keeney M, Lin TH, Pajarinen J, Barcay K, Waters H, Egashira K, Yang F, Goodman S. Mutant monocyte chemoattractant protein 1 protein attenuates migration of and inflammatory cytokine release by macrophages exposed to orthopedic implant wear particles. J Biomed Mater Res A 2014;102:3291–3297.
20. Jiang X, Sato T, Yao Z, Keeney M, Pajarinen J, Lin TH, Loi F, Egashira K, Goodman S, Yang F. Local delivery of mutant CCL2 protein-reduced orthopaedic implant wear particle-induced osteolysis and inflammation in vivo. J Orthop Res 2016;34:58–64.
21. Keeney M, Waters H, Barcay K, Jiang X, Yao Z, Pajarinen J, Egashira K, Goodman SB, Yang F. Mutant MCP-1 protein delivery from layer-by-layer coatings on orthopedic implants to modulate inflammatory response. Biomaterials 2013;34:10287–10295.
22. Pajarinen J, Tamaki Y, Antonios JK, Lin TH, Sato T, Yao Z, Takagi M, Konttinen YT, Goodman SB. Modulation of mouse macrophage polarization in vitro using IL-4 delivery by osmotic pumps. J Biomed Mater Res A 2015;103:1339–1345.
23. Ma T, Huang Z, Ren PG, McCally R, Lindsey D, Smith RL, Goodman SB. An in vivo murine model of continuous intramedullary infusion of polyethylene particles. Biomaterials 2008;29:3738–3742.
24. Ren PG, Irani A, Huang Z, Ma T, Biswal S, Goodman SB. Continuous infusion of UHMWPE particles induces increased bone macrophages and osteolysis. Clin Orthop Relat Res 2011;469:113–122.
25. Gan L, Wang J, Tache A, Valiquette N, Deporter D, Pilliar R. Calcium phosphate sol-gel-derived thin films on porous-surfaced implants for enhanced osteoconductivity. Part II: Short-term in vivo studies. Biomaterials 2004;25:5313–5321.
26. Spoor CF, Zonneveld FW, Macho GA. Linear measurements of cortical bone and dental enamel by computed tomography: Applications and problems. Am J Phys Anthropol 1993;91:469–484.
27. Mikić B, van der Meulen MC, Kingsley DM, Carter DR. Long bone geometry and strength in adult BMP-5 deficient mice. Bone 1995; 16:445–454.
28. Brown BN, Sicari BM, Badylak SF. Rethinking regenerative medicine: A macrophage-centered approach. Front Immunol 2014;5: 510.
29. Bendixen AC, Shevde NK, Dienger KM, Willson TM, Funk CD, Pike JW. IL-4 inhibits osteoclast formation through a direct action on osteoclast precursors via peroxisome proliferator-activated receptor gamma 1. Proc Natl Acad Sci USA 2001;98:2443–2448.
30. Silfverswärd CJ I, Penno H, Frost A, Nilsson O, Ljunggren O. Expression of markers of activity in cultured human osteoblasts: Effects of interleukin-4 and interleukin-13. Scand J Clin Lab Invest 2010;70:338–342.
31. Ura K, Morimoto I, Watanabe K, Saito K, Yanagihara N, Eto S. Interleukin (IL)−4 and IL-13 inhibit the differentiation of murine osteoblastic MC3T3-E1 cells. Endocr J 2000;47:293–302.
32. Claes L, Recknagel S, Ignatius A. Fracture healing under healthy and inflammatory conditions. Nat Rev Rheumatol 2012;8:133–143.
33. Gibon E, Yao Z, Rao AJ, Zwingenberger S, Batke B, Valladares R, Smith RL, Biswal S, Gambhir SS, Goodman SB. Effect of a CCR1 receptor antagonist on systemic trafficking of MSCs and polyethylene particle-associated bone loss. Biomaterials 2012;33:3632–3638.